Available online at www.sciencedirect.com
SCIENCE DIRECT®
International Journal of Heat and Mass Transfer 49 (2006) 4106–4115
International Journal of HEAT and MASS TRANSFER
www.elsevier.com/locate/ijhmt

Influence of natural convection on the melting of ice block surrounded by water on all sides

Zdravko Virag [a,*], Marija Živić [b], Antun Galović [a]

[a] Faculty of Mechanical Engineering and Naval Architecture, University of Zagreb, I. Lučića 5, 10 000 Zagreb, Croatia
[b] Mechanical Engineering Faculty, Trg I.B. Mažuranić 18, University of Osijek, 35 000 Slavonski Brod, Croatia

Received 25 July 2005
Available online 27 June 2006

Abstract

The ice block at initial temperature $T_{is} = 0$ °C is fixed at the center of a long, prismatic enclosure with isothermal vertical walls and insulated horizontal walls. The enclosure is completely filled with water at initial temperature $T_{il} = 0$ °C. Six numerical simulations were performed by varying vertical wall temperatures from $T_W = 2$ to 12 °C (range of Rayleigh number from 4.22×10^6 to 2.28×10^7). In the case of $T_W > 8$ °C the ice melts faster from above and for $T_W < 8$ °C from below. In the case of $T_W = 8$ °C, two vortices are separated by nearly vertical 4 °C isotherm and the average Nusselt number remains constant during the convection dominated regime.
© 2006 Elsevier Ltd. All rights reserved.

Keywords: Ice melting; Natural convection; Rectangular enclosure; Finite volume method

1. Introduction

Melting and freezing are phase change phenomena that have become an indispensable part of many technological processes like the manufacturing of metal alloys, glass and crystals, continuous casting, welding and purification of metals. The processes of melting and solidification belong to the class of moving or free boundary problems. The essential and common feature of these problems is the existence of a time and space dependent phase boundary, whose position cannot be identified in advance, but has to be determined as an important constituent of the solution. The existence of the moving boundary introduces a non-linear character to this type of problems, and causes a lot of computational difficulties in the seeking of solution. Nowadays, these problems are usually solved by numerical techniques. There are two main groups of numerical methods for solving the moving boundary problems: front tracking methods and fixed spatial grid methods. A review of the methods is given by Yao and Prusa [1]. Fukusako and Yamada [2] have presented an extensive summary of the work carried out on water freezing and ice melting problems. The literature concerning the problem of ice melting driven by natural convection in the presence of maximum density appears to be mostly restricted to the cylindrical geometry [3,4]. This problem is dealt with in many applications such as ice thermal storage techniques for air-conditioning, or the production of ice. Experimental and numerical studies of water freezing by convection involving maximum density inside rectangular cavities are relatively extensive [5–7]. However, few studies have been carried out on ice melting in an enclosure for situations in which the density maximum is important. Vieira et al. [8] presented a numerical and experimental investigation into the effect of maximum density of water on the melting of a vertical ice layer in a rectangular enclosure.

In this paper the influence of natural convection during melting of a long ice block in a rectangular enclosure with isothermal vertical walls filled with water is analyzed numerically. Six simulations were performed by varying hot wall temperatures from 2 to 12 °C.

* Corresponding author.
E-mail addresses: zdravko.virag@fsb.hr (Z. Virag), marija.zivic@sfsb.hr (M. Živić).

0017-9310/$ - see front matter © 2006 Elsevier Ltd. All rights reserved.
doi:10.1016/j.ijheatmasstransfer.2006.04.007

Nomenclature

a	thermal diffusivity
a_E, a_N, a_S, a_W, a_P	coefficients in the difference equation
B	length of the rectangular cavity
c	specific heat capacity
f	solid fraction
g	gravitational acceleration
h_L	latent heat of fusion
H	height of the rectangular cavity
k	thermal conductivity
L	characteristic length
p	pressure
$\dot{Q}$	heat transfer rate
t	time
T	temperature
$\dot{U}$	rate of change of water internal energy
u, v	velocity components in Cartesian coordinates x, y
V_{init}	initial volume of ice
V_s	solidified volume, m^3
W	width of the rectangular cavity
x, y	Cartesian coordinates,
$x^0 = \frac{x}{W}$	dimensionless x coordinate
$y^0 = \frac{y}{W}$	dimensionless y coordinate
μ	dynamic viscosity
v	kinematic viscosity
ρ	density
ρ_0	constant density of liquid
ρ_{max}	maximal density of water at 4 °C
$(\Delta\rho)_{max}$	difference between maximum and minimum density in the considered problem
$Nu_W = \frac{\dot{Q}_W \cdot W}{k_1 \cdot \Delta T_1 \cdot H \cdot B}$	average Nusselt number
$Pr = \frac{v_1}{a_1}$	Prandtl number
$\dot{Q}^0_{ice} = \frac{\dot{Q}_{ice} \cdot W}{k_1 \cdot \Delta T_1 \cdot H \cdot B}$	dimensionless heat transfer rate from water to ice
$Ra = \frac{g \cdot H^3 \cdot (\Delta\rho)_{max}}{v_1 \cdot a_1 \cdot \rho_{max}}$	Rayleigh number
$Ste = \frac{c_1 (T_W - T_m)}{h_L}$	Stefan number
$\tau = \frac{a_1 \cdot t \cdot Ste}{H^2}$	dimensionless time
$\tau_M = Ste \cdot \frac{a_1 \cdot t_M}{H^2}$	dimensionless total time of melting

Subscripts

i	initial
m	melting
s	solid
l	liquid
P	at the node P
W	west boundary
N	north boundary
S	south boundary
E	east boundary
1	clockwise
2	counterclockwise

Superscript

0	at previous time step

The considered problem is of interest because of its fundamental nature. The goal of the work is to obtain a physical image and to identify main regimes in the melting process of an ice block when it is surrounded by water on all sides.

2. Mathematical model

Unsteady two-dimensional melting of ice is governed by the basic laws represented by the continuity, momentum and energy equations and by the following assumptions: the liquid phase is incompressible and the Boussinesq approximation is met, the flow is laminar, and viscous dissipation is neglected. The mathematical model takes the form

$$\frac{\partial u}{\partial x} + \frac{\partial v}{\partial y} = 0 \tag{1}$$

$$\rho_0 \frac{\partial u}{\partial t} + \rho_0 \left(u \frac{\partial u}{\partial x} + v \frac{\partial u}{\partial y} \right) = -\frac{\partial p}{\partial x} + \mu \left(\frac{\partial^2 u}{\partial x^2} + \frac{\partial^2 u}{\partial y^2} \right) \tag{2}$$

$$\rho_0 \frac{\partial v}{\partial t} + \rho_0 \left(u \frac{\partial v}{\partial x} + v \frac{\partial v}{\partial y} \right) = g(\rho_0 - \rho) - \frac{\partial p}{\partial y} + \mu \left(\frac{\partial^2 v}{\partial x^2} + \frac{\partial^2 v}{\partial y^2} \right) \tag{3}$$

$$\rho_0 c \frac{\partial T}{\partial t} + \rho_0 c \left(u \frac{\partial T}{\partial x} + v \frac{\partial T}{\partial y} \right) = k \left(\frac{\partial^2 T}{\partial x^2} + \frac{\partial^2 T}{\partial y^2} \right) + \rho_s h_L \frac{\partial f}{\partial t} \tag{4}$$

Boundary conditions for the considered problem include conditions at the solid impermeable isothermal or insulated wall and the boundary condition at the solid–liquid interface. At the impermeable wall both velocity components are equal to zero. At the isothermal wall the boundary temperature is prescribed, while at the insulated wall the normal derivative of temperature is equal to zero.

At the solid–liquid interface the temperature is constant and equal to the melting temperature T_m. If the interface velocity is negligible, the Stefan condition at the interface follows from the energy equation, Eq. (4), in the form

$$k_s \left. \frac{\partial T}{\partial n} \right|_s - k_l \left. \frac{\partial T}{\partial n} \right|_l = \rho_s h_L \frac{\partial n}{\partial t} \tag{5}$$

where the indices l and s refer to the liquid and solid phase, respectively, and n is the coordinate normal to the phase boundary.

3. Numerical method

In order to solve the equations of mathematical model, the finite volume method, Patankar [9], using the fixed

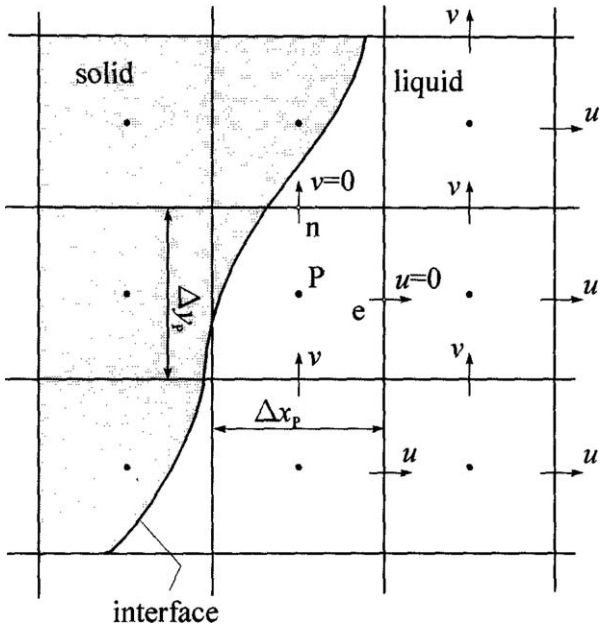

Fig. 1. A part of computational domain.

rectangular grid has been adopted. The values of the pressure and temperature field are computed at the central nodes. The nodes for the u-velocity component are staggered in the x-direction, while the nodes for the v–velocity component are staggered in the y-direction as shown in Fig. 1.

The governing equations are discretized using the exponential differencing scheme [10] for the spatial derivatives and the fully implicit scheme for the time integration. For the pressure–velocity coupling the SIMPLER algorithm is used. As the adopted finite volume method is well known, only the details concerning the phase change term in the energy equation and the implementation of the Stefan condition have been given here. Discretized form of Eq. (4) is

$$a_P T_P = a_E T_E + a_W T_W + a_N T_N + a_S T_S + a_{P0} T_P^0 + \rho_s h_L \frac{V_s - V_s^0}{\Delta t} \quad (6)$$

where V_s^0 and V_s are the values of the control volume solidified part at the times t and $t + \Delta t$, respectively. The coefficients a_P, a_E, a_N, a_W and a_S depend on the adopted differencing scheme and the coefficient a_{P0} originates from the unsteady term. Fig. 1 shows a part of computational domain containing a solid–liquid interface. If during the considered time step the control volume lies in the liquid or in the solid phase, the last term of Eq. (6) is equal to zero and the energy equation defines the temperature T_P of the control volume. If the interface passes through the control volume, the temperature T_P of the volume is set to the melting temperature T_m, while the value of the solidified volume V_s is calculated from Eq. (6). At the initial time, the values of V_s^0 are obtained on the basis of the initially prescribed temperature. For a control volume with the temperature higher than T_m, the value of V_s^0 is set to $V_s^0 = 0$, and in other case the volume is solidified with $V_s^0 = \Delta x_P \Delta y_P$. For each time step the calculation starts with the assumed value of V_s, using the constraint $0 \leqslant V_s \leqslant \Delta x_P \Delta y_P$ and the final value of V_s is calculated through the iterative procedure. The iterative procedure ends when the assumptions for V_s for all control volumes are confirmed, and the prescribed accuracy of calculations for all governing equations is achieved. The implementation of boundary conditions for velocity field is reduced to the examination of V_s. For a control volume in which a phase change occurs ($V_s > 0$), the velocity components at the volume faces are set to zero, while the coefficients defined by the differencing scheme stay unchanged. It is well known that natural convection in water has a special feature due to the water anomaly. The density variation with the temperature in the range 0–20 °C can be approximated by the following equation (see, for example, [11]):

$$\{\rho\}_{kg/m^3} = \frac{999.8396}{1 + k_1\{T\}_{^\circ C} + k_2\{T\}_{^\circ C}^2 + k_3\{T\}_{^\circ C}^3 + k_4\{T\}_{^\circ C}^4} \quad (7)$$

where $k_1 = -0.6789645 \times 10^{-4}$, $k_2 = 0.907294338 \times 10^{-5}$, $k_3 = -0.96456812 \times 10^{-7}$, $k_4 = 0.873702983 \times 10^{-9}$.

The non-linear density–temperature variation leads to significantly more complicated natural convection flow patterns than in the case of the linear one.

4. Results and discussion

4.1. Problem 1 – Melting of vertical ice layer in a rectangular cavity

A numerical investigation, presented in this section, is concerned with the melting problem of a vertical ice layer in the presence of the horizontal temperature gradients experimentally investigated by Vieira [12]. The considered melting process occurs inside a rectangular cavity ($H = 0.0935$ m, $L = 0.187$ m, shown in Fig. 2), with isothermal vertical walls maintained at different temperatures. Initially, half of cavity volume is filled with water, while the other half is filled with ice, both at the melting temperature ($T_{is} = T_{il} = T_m$). The northern and southern walls are adiabatic. Eastern wall is maintained at melting temperature

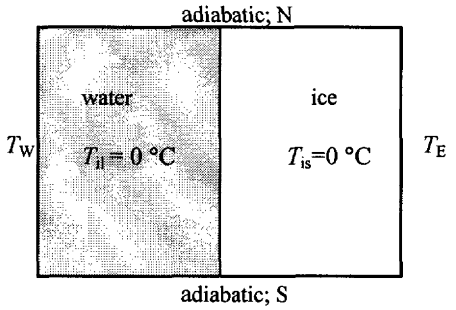

Fig. 2. Schematic view of vertical ice layer melting process.

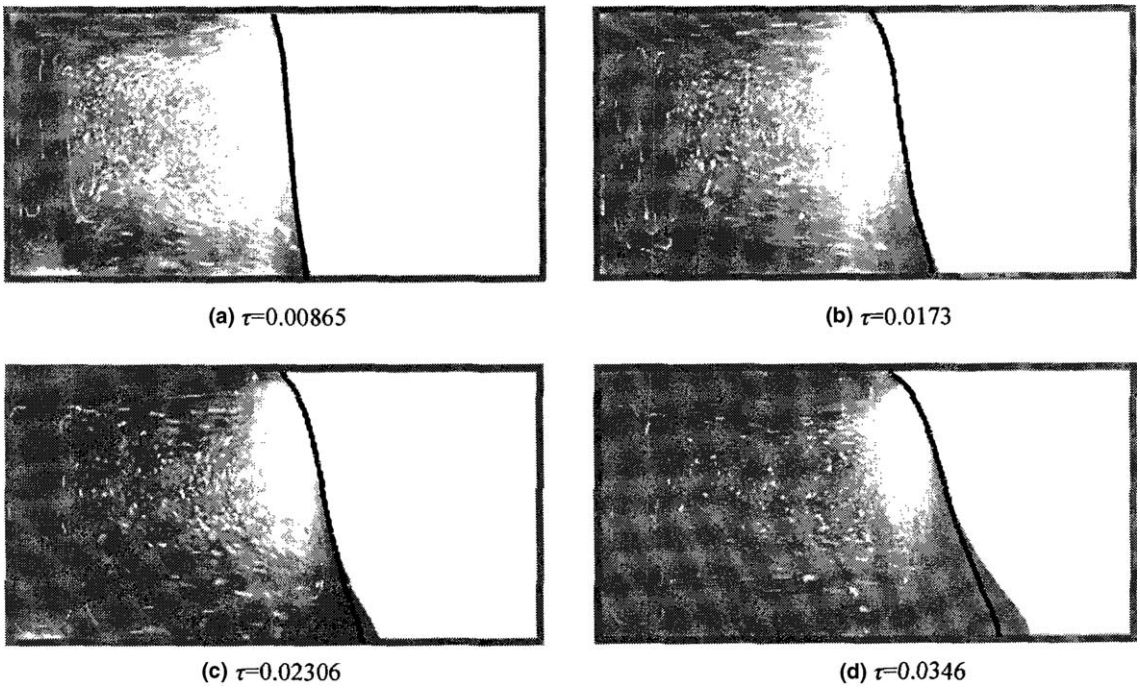

Fig. 3. Interface shapes of vertical ice layer at selected times – numerical results (drawn black line) compared with experimental results (presented by the photograph of the cavity).

$T_E = T_m = 0$ °C. At time $t = 0$, the western wall is abruptly heated at the temperature $T_W = 8$ °C and maintained at this temperature thereafter. The principal dimensionless groups are: $Pr = 10.71$; $Ra = 4.98 \times 10^6$; $Ste = 0.1$.

Numerical computation is performed on the non-uniform 160×100 control volume (CV) grid. The total dimensionless integration time was $\tau = 0.046$ and the integration time step was $\Delta\tau = 1.6 \times 10^{-7}$.

Fig. 3 shows the comparison of interface shapes obtained in experiment and in numerical simulation at four different times. At the beginning of melting process the numerical results are almost identical with experimental ones, while toward the end of the process the certain discrepancy has been increasing at the bottom of the cavity. The obtained results confirm the validity of the adopted mathematical model and numerical method.

4.2. Problem 2 – Melting of ice block in a rectangular enclosure filled with water

The considered problem is schematically shown in Fig. 4. The analyzed problem is the melting of a long ice block at initial temperature $T_{is} = 0$ °C. The ice block is fixed at the center of a long, prismatic enclosure completely filled with water at initial temperature $T_{il} = 0$ °C. The problem is symmetrical with respect to the vertical midplane. It is supposed that the enclosure is sufficiently long in the direction normal to the plane of the enclosure for the motion to be assumed to be two-dimensional. The northern and southern walls are adiabatic, whereas the eastern boundary is the symmetry plane. Western wall is isothermal, maintained at a constant temperature T_W. Initially, the volume of ice is 1/8, and the volume of water is 7/8 of the cavity volume.

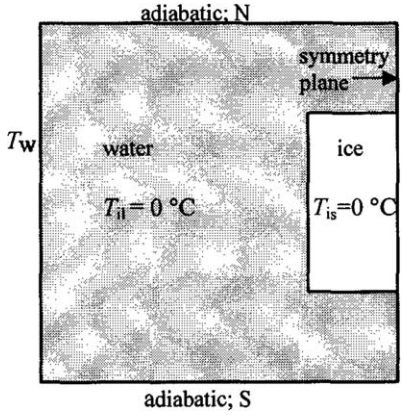

Fig. 4. Schematic view of ice block melting problem.

Six simulations were performed covering a wide range of hot wall temperatures T_W (2, 4, 6, 8, 10 and 12 °C). Numerical simulations are conducted on the non-uniform 160×160 control volume grid, shown in Fig. 5, which has been refined in the ice region. Numerical integration was being carried out till the end of the process of ice block melting.

The principal dimensionless group (Pr, Ra, Ste), together with the values of dimensionless melting time τ_M (the time needed for the process of ice melting to be finished) are summarized in Table 1.

It can be seen that the longest dimensionless melting time is required in the case of $T_W = 8$ °C. Fig. 6 shows the interface shapes of ice block at selected times when

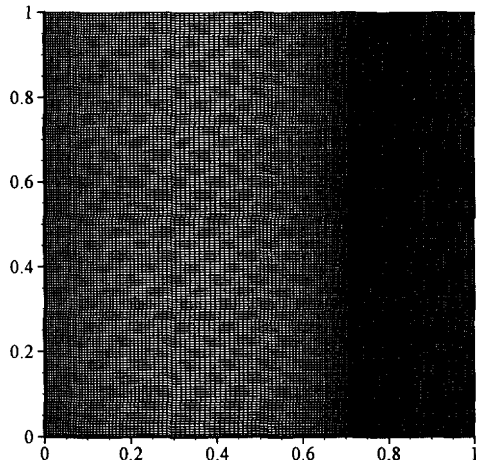

Fig. 5. The adopted grid.

Table 1
The values of dimensionless groups and dimensionless melting time for all considered cases

	Ste	*Pr*	*Ra*	τ_M
$T_W = 2$ °C	0.0253	12.96	4.224×10^6	0.01292
$T_W = 4$ °C	0.0506	12.56	5.756×10^6	0.01287
$T_W = 6$ °C	0.0759	12.06	5.906×10^6	0.01508
$T_W = 8$ °C	0.1012	11.58	5.680×10^6	0.01773
$T_W = 10$ °C	0.1265	11.18	1.295×10^7	0.01488
$T_W = 12$ °C	0.1518	10.89	2.279×10^7	0.01321

the remaining part of ice volume is 75%, 50%, 25% and 10% of the initial volume. Table 2 contains numerical values of dimensionless time for selected cases shown in Fig. 6. It is clear from Fig. 6 that in the case of $T_W < 8$ °C, the ice is melting faster from below, and for $T_W > 8$ °C from above. For $T_W = 8$ °C the ice block is melting almost uniformly from all sides.

In the cases of $T_W = 2$, 4 and 6 °C, the average Nusselt number decreases smoothly in time, while in the cases of $T_W = 8$, 10 and 12 °C, the average Nusselt number curves change abruptly at certain time. That will be explained by an analysis of velocity and temperature fields. A detailed

Table 2
Dimensionless time τ corresponding to a certain remaining part of ice volume

	$V = 0.75V_{init}$	$V = 0.5V_{init}$	$V = 0.25V_{init}$	$V = 0.1V_{init}$
$T_W = 4$ °C	0.0030	0.0055	0.0085	0.0108
$T_W = 6$ °C	0.0034	0.0064	0.0097	0.0121
$T_W = 8$ °C	0.0044	0.0086	0.0128	0.0151
$T_W = 10$ °C	0.0048	0.0079	0.0107	0.0126
$T_W = 12$ °C	0.0048	0.0070	0.0094	0.0113

analysis for the case of $T_W = 10$ °C is carried out, followed by a discussion of other cases. The results are presented in the form of streamlines and the 4 °C isotherm shown in Figs. 7 and 8. The 4 °C isotherm, when superimposed on the streamline pattern, gives the location of the density maximum and separates two vortices: the counterclockwise (in the region of water temperature between 0 °C and 4 °C – dark gray in Figs. 7 and 8) and the clockwise (in the region of water temperature greater than 4 °C, light gray in Figs. 7 and 8). In these figures the ice region is white, and the 4 °C isotherm is the white line between two gray regions.

Taking into account that the ice temperature is equal to the melting temperature all the time, the equation of energy balance for the whole system states

$$\dot{Q}_W = \dot{U} + \dot{Q}_{ice} \tag{8}$$

It is worth to note that the heat transfer rate from water to ice $\dot{Q}_{ice}$ is equal to the rate of heat sink due to ice melting. In the case of two vortices, as depicted in Fig. 9, the heat transfer rate at the hot wall may be divided into two parts representing the heat transfer rate between the wall and clockwise vortex and between the wall and counterclockwise vortex in the form $\dot{Q}_W = \dot{Q}_{W1} + \dot{Q}_{W2}$, or in the dimensionless form $Nu_W = Nu_{W1} + Nu_{W2}$. The heat transfer rate between the water and ice, as well as the rate of change of water internal energy may also be divided into contributions from the clockwise and counterclockwise vortices in the form $\dot{Q}_{ice} = \dot{Q}_{ice1} + \dot{Q}_{ice2}$ and $\dot{U} = \dot{U}_1 + \dot{U}_2$. It is clear that the following relations are valid for the energy

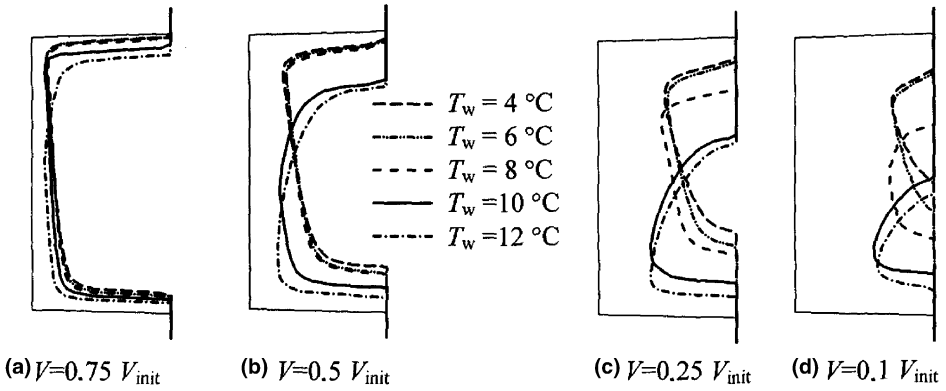

Fig. 6. Interface shapes of ice block at selected times.

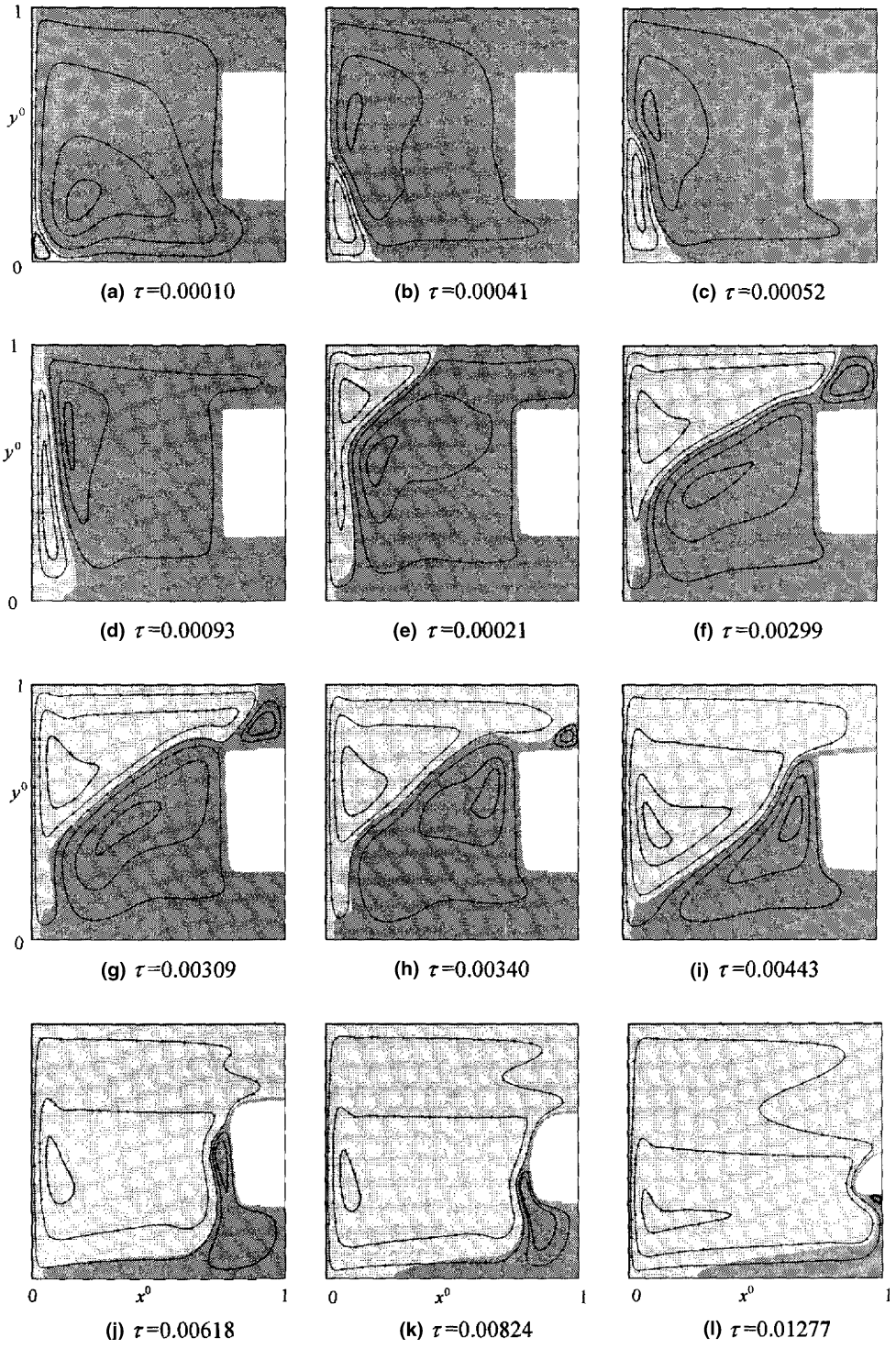

Fig. 7. Streamlines for the case $T_W = 10$ °C at selected dimensionless times.

balances for the volumes occupied by the clockwise and counterclockwise vortices.

$$\dot{Q}_{W1} = \dot{U}_1 + \dot{Q}_{ice1} + \dot{Q}_{12} \quad \text{and} \quad \dot{Q}_{W2} + \dot{Q}_{12} = \dot{U}_2 + \dot{Q}_{ice2} \tag{9}$$

The terms $\dot{Q}_{W1}$, $\dot{Q}_{W2}$, $\dot{Q}_{ice1}$ and $\dot{Q}_{ice2}$ are calculated numerically as sums of heat transfer rates through the control volume faces at the hot wall and ice surface. Control volumes with positive vertical velocity component near the hot wall, and with negative vertical velocity component near the ice surface belong to the clockwise vortex. For the counterclockwise vortex it is the opposite case: near the hot wall the vertical velocity component is negative and near the ice surface it is positive. Fig. 10a shows the time evolution of the average Nusselt number at the hot wall for three

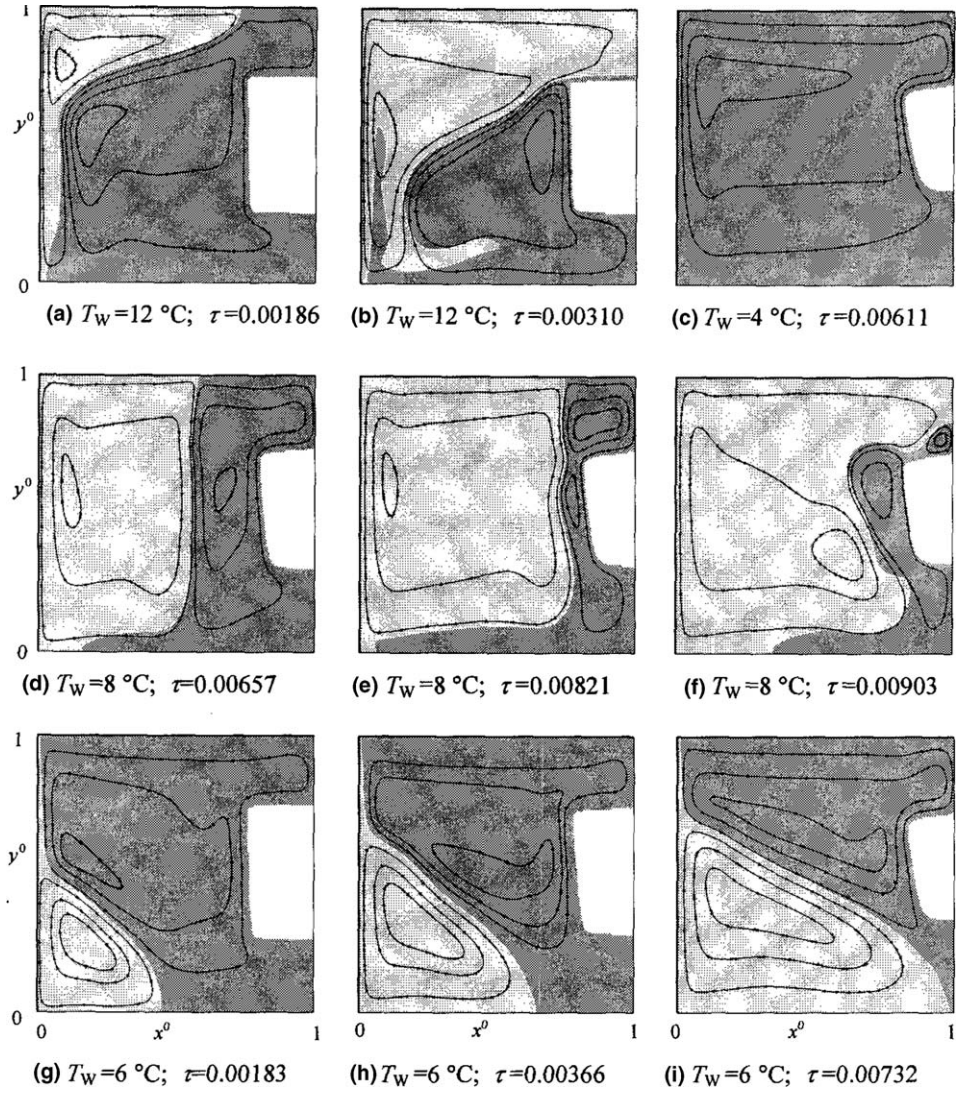

Fig. 8. Streamlines for the cases $T_W = 12$, 8, 6 and 4 °C at selected dimensionless times.

cases of $T_W = 2$, 4 and 6 °C, and Fig. 10b for three cases of $T_W = 8$, 10 and 12 °C. Fig. 11a–d shows values of average

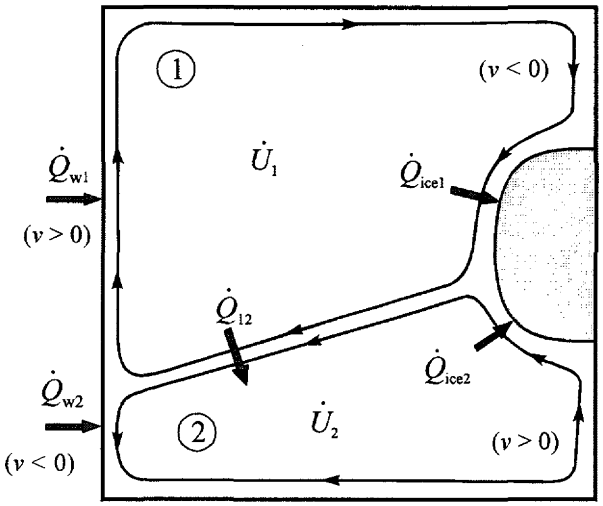

Fig. 9. Scheme of two vortices in the flow field.

Nusselt number Nu_W, Nu_{W1} and Nu_{W2} at the hot wall, and dimensionless heat transfer rates $\dot{Q}^0_{ice}$, $\dot{Q}^0_{ice1}$ and $\dot{Q}^0_{ice2}$ at the ice surface for the cases $T_W = 10$, 12, 8 and 6 °C.

The detailed description of the particular cases follows.

4.2.1. Case $T_W = 10$ °C

From the time evolution of the average Nusselt number at the hot wall, one can distinguish the conduction and convection dominated regimes of heat transfer. During the convection dominated regime the contribution of clockwise vortex and counterclockwise vortex in ice melting may be estimated from the time evolution of the heat transfer rates shown in Fig. 11a. The pictures of streamlines and 4 °C isotherm at selected times shown in Fig. 7a–l can explain these regimes.

4.2.1.1. An initial pure conduction regime. At the very beginning of the melting process ($\tau < 1.72 \times 10^{-5}$ that cannot be seen in Fig. 11a), heat transfer is dominated by conduction. The isotherms are almost parallel to the hot wall. There is

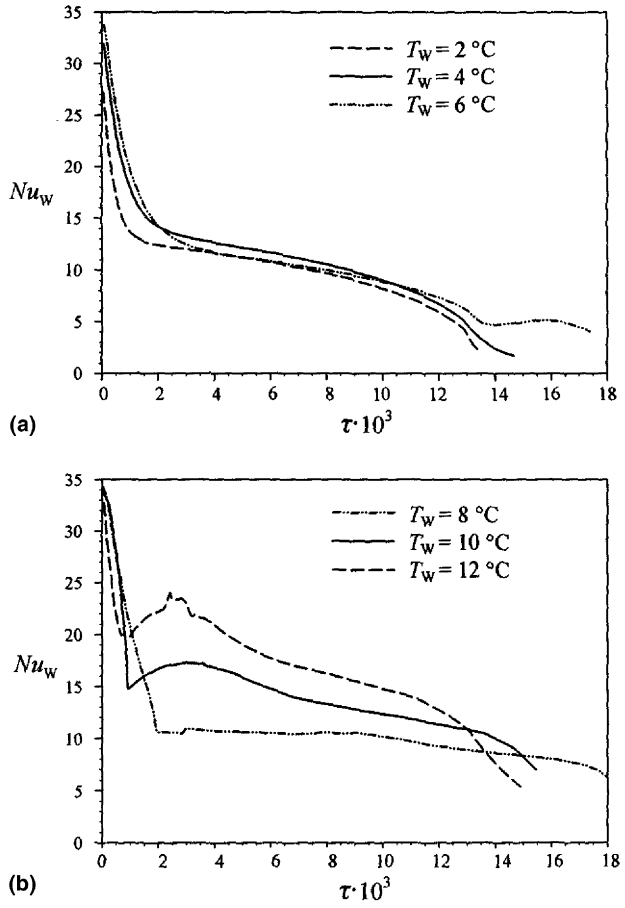

Fig. 10. Time evolution of the average Nusselt number at the hot wall for cases (a) $T_W < 8$ °C and (b) $T_W \geqslant 8$ °C.

no significant motion of the water and there is no melting of ice yet.

4.2.1.2. A transition regime. The transition regime begins with the appearance of a small clockwise vortex at the bottom of the hot wall and a counterclockwise vortex near the ice block. The counterclockwise vortex is very weak, and takes place almost in the entire region of the water, as shown in Fig. 7a. It is clear that the heat transfer rate is more intensive at the upper portion of the hot wall due to the larger temperature gradient than in the lower portion where the clockwise vortex exists. As the clockwise vortex grows, as shown in Fig. 7b–d, the average Nusselt number at the hot wall sharply decreases, as shown in Fig. 11a. At the end of this regime the clockwise vortex has grown over the entire height of the hot wall, Nu_{W2} becomes equal to zero ($\tau = 0.00093$) and the average Nusselt number reaches a local minimum in a certain time. During this regime the ice is melting slowly, from below.

4.2.1.3. A regime of developed convection. This regime can be divided into three sub-regimes. The first sub-regime, which lasts approximately up to $\tau = 0.00309$, is characterized by the expansion of clockwise vortex on the account of the counterclockwise one, as shown in Fig. 7e. As the clockwise vortex expands, the intensity of natural convection rises and the heat transfer rate at the hot wall increases, as shown in Fig. 11a. At the end of this sub-regime the clockwise vortex is expanded close to the ice region, and the heat transfer rate at the hot wall has reached a local maximum. At the end of this sub-regime the counterclockwise vortex is divided into two vortices: a smaller one placed above the ice and a bigger one placed beside and below the ice block, as shown in Fig. 7f and g. During this sub-regime the clockwise vortex is not in the contact with the ice ($\dot{Q}^0_{ice1}$ is equal to zero, as shown in Fig. 11a), so the ice is still melted faster from below than from above.

The second sub-regime begins when the warm water starts entering the space above the ice block, as it is shown in Fig. 7g and h. At the beginning of this sub-regime the heat transfer rate between water and ice is abruptly changed due to contact of hot water from the clockwise vortex and ice, as it is shown in Fig. 11a, so the ice is melting faster from above than from below. At the top of the ice a thin boundary layer is formed, and at the end of this sub-regime the horizontal temperature stratification appears in the water in the upper portion of the cavity. The counterclockwise vortex still occupies nearly half of the cavity volume.

During the third sub-regime, the clockwise vortex prevails over the counterclockwise one and the ice is melting mainly from above because the thermal boundary layer becomes thinner and the heat transfer rate from water to ice increases. Fig. 7k shows streamlines and the 4 °C isotherm at $\tau = 0.00824$. After this time, the warm water (clockwise vortex) enters the region below the ice, as shown in Fig. 7l. The ice is completely melted at $\tau = 0.0148$, as can be seen from Fig. 11a.

4.2.2. Case $T_W = 12$ °C

This case is qualitatively very similar to the case of $T_W = 10$ °C. The ice block is melting faster than in the previous case due to the bigger temperature difference between the hot wall and the ice.

Fig. 8a and b shows streamlines and the regions of two vortices at two instants, one before and the other after the warm water enters the space above the ice. After the former, the ice block is melting faster from above than from below, as in a previous case. Fig. 11b shows the time evolutions of the Nusselt number and dimensionless heat transfer rates $\dot{Q}^0_{ice}$, $\dot{Q}^0_{ice1}$ and $\dot{Q}^0_{ice2}$ that are very similar to the case of $T_W = 10$ °C.

4.2.3. Case $T_W = 8$ °C

In this case, the transition regime (growing of the clockwise vortex up to the entire height of the hot wall) ends at $\tau = 0.0021$ and after that, the two vortices are separated by nearly vertical 4 °C isotherm. In the next regime, the clockwise vortex expands, while the 4 °C isotherm remains nearly vertical as it is shown in Fig. 8d and e.

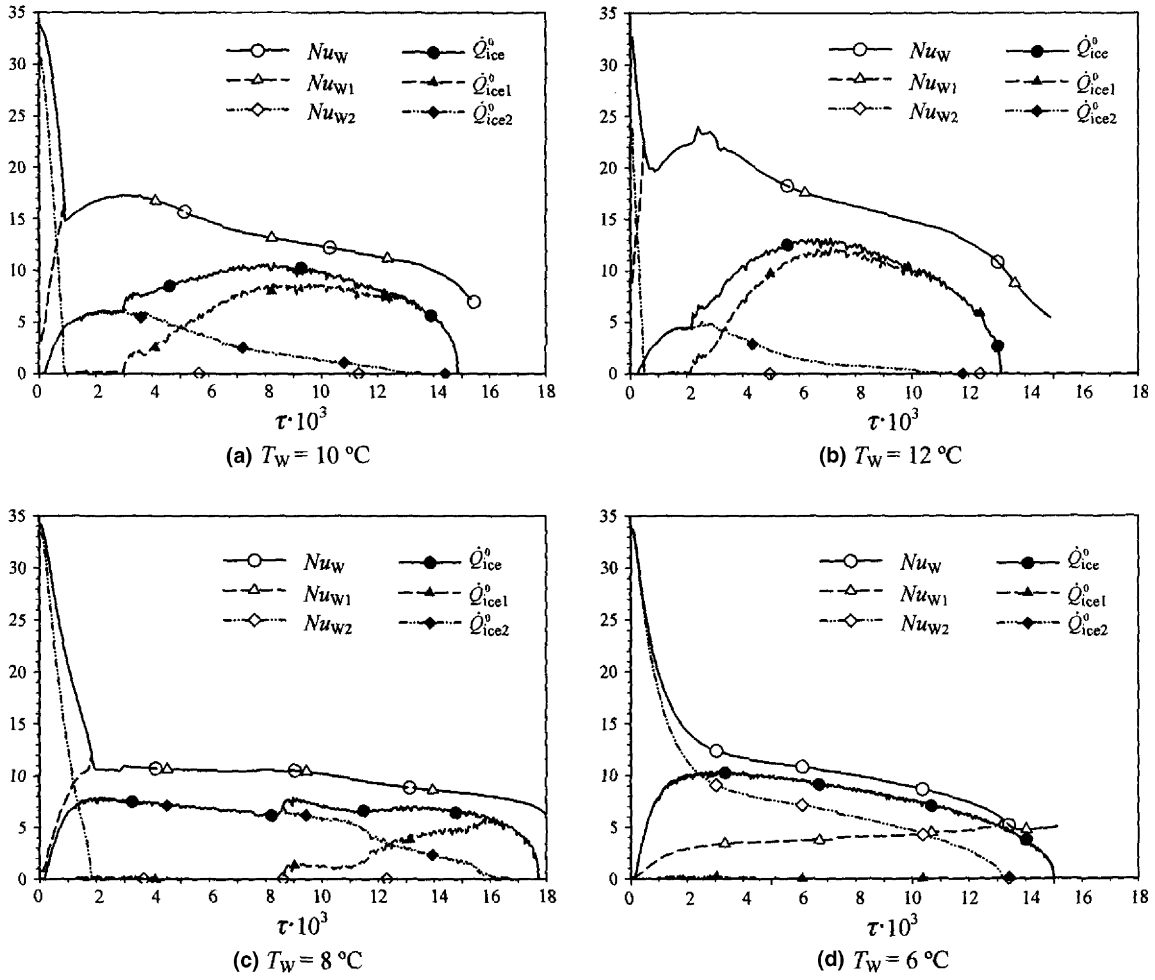

Fig. 11. Time evolution of the average Nusselt number at the hot wall for $T_W = 10, 12, 8, 6$ °C.

The temperature drop is 4 °C in both vortices, the sum of their widths is constant, so their thermal resistance is independent of the individual sizes of vortices. Because of that the average Nusselt number stays nearly constant until the clockwise vortex is spread close to the ice block, as it can be seen in Fig. 11c. When the clockwise vortex is spread close to the ice block, warm water tends to enter the space above and below the ice block, as shown in Fig. 8f. That is why the ice melting is nearly uniform from all sides.

4.2.4. Case $T_W = 6$ °C

In this case the clockwise vortex grows along the vertical wall during almost the entire melting process (the heat transfer rate Nu_{W2} becomes equal to zero at $\tau = 0.01329$, while total melting time $\tau_M = 0.01508$). It expands faster to the right than upwards so the counterclockwise vortex is in a direct contact with both the hot wall and the ice block. That is why the ice block is melting faster from below than from above. Fig. 8g–i illustrates the clockwise vortex expansion. The Nusselt number decreases smoothly with the decrease of the contact area between counterclockwise vortex and the hot wall, as shown in Fig. 11d.

4.2.5. Cases $T_W = 2$ °C and 4 °C

In these cases only the counterclockwise vortex exists and it is melting the ice block faster from below than from above. The Nusselt number smoothly decreases in time and the dimensionless melting time is nearly equal in both cases.

5. Conclusions

In the case of $T_W > 8$ °C the melting process may be divided into three typical successive regimes: an initial pure conduction regime, a transition regime and a convection dominated regime. The former regime can be divided into three sub-regimes. The first sub-regime is characterized by the expansion of the clockwise vortex on the account of the counterclockwise one. As the clockwise vortex expands the heat transfer rate at the hot wall increases. At the end of this sub-regime, the clockwise vortex is expanded close to the ice block, the heat transfer rate at the hot wall reaches a local maximum and the ice is still melting faster from below than from above. The second sub-regime starts when the warm water enters the space above the ice so that the ice starts melting faster from

above than from below. During the third sub-regime, the clockwise vortex completely prevails over the counterclockwise one, and the ice is again melting faster from above than from below. In the case of $T_W = 8\ ^\circ C$ the vortices are separated by nearly vertical 4 °C isotherm, and the average Nusselt number stays constant during the time interval. In the case of $T_W < 8\ ^\circ C$, the clockwise vortex expands faster to the right than upwards, so the ice is melting faster from below than from above all the time.

References

[1] L.S. Yao, J. Prusa, Melting and Freezing, Advances in Heat Transfer, vol. 19, Academic Press, San Diego, 1989, pp. 1–95.

[2] S. Fukusako, M. Yamada, Recent advances in research on water-freezing and ice-melting problems, Exp. Therm. Fluid Sci. 6 (1993) 90–105.

[3] H. Rieger, H. Beer, The melting process of ice inside a horizontal cylinder: effects of density anomaly, J. Heat Transfer 108 (1986) 166–173.

[4] T.J. Scanlon, M.T. Stickland, An experimental and numerical investigation of natural convection melting, Int. Commun. Heat Mass Transfer 28 (2001) 181–190.

[5] S.L. Braga, R. Viskanta, Effect of density extremum on the solidification of water on a vertical wall of rectangular cavity, Exp. Therm. Fluid Sci. 5 (1992) 703–713.

[6] T.A. Kowalewski, M. Rebow, Freezing of water in a differentially heated cubic cavity, Int. J. Comput. Fluid Dyn. 11 (1999) 193–210.

[7] P.H. Oosthuizen, The development of convective motion in a bottom heated square enclosure containing ice and water, Int. J. Therm. Sci. 40 (2001) 145–151.

[8] G.R. Vieira, S.L. Braga, D. Gobin, Convective melting of ice near 4 °C, in: 5th World Conf. on Exp. Heat Transfer, Fluid Mech. and Thermodynamics, Thessaloniki, 24–28 September 2001, vol. 3, pp. 2113–2118.

[9] S.V. Patankar, Numerical Heat Transfer and Fluid Flow, Hemisphere, McGraw-Hill, New York, 1980.

[10] D.B. Spalding, A. Novel, Finite-difference formulation for differential expression involving both first and second derivatives, Int. J. Numer. Methods Eng. 4 (1972) 551–559.

[11] P. Vasseur, L. Robillard, Transient natural convection heat transfer in a mass of water cooled through 4 °C, Int. J. Heat Mass Transfer 23 (1980) 1195–1205.

[12] G. Vieira, Análise numérico-experimental do processo defusao de substâncias apresentando um máximo de densidade, PhD thesis, Pontifícia Universidade Católica do Rio de Janeiro, Rio de Janeiro, Brasil, 1998.